Article

Not peer-reviewed version

The Curvature Parameter of the Symmetry Energy and a Modified Polytropic Equation of State

Ilona Bednarek , Wiesław Olchawa , Jan Sładkowski * , Jacek Syska

Posted Date: 2 February 2026

doi: 10.20944/preprints202602.0114.v1

Keywords: symmetry energy; polytropic equation of state; neutron stars

Preprints.org (www.preprints.org) | NOT PEER-REVIEWED | Posted: 2 February 2026 doi:10.20944/preprints202602.0114.v1

Article

The Curvature Parameter of the Symmetry Energy and a Modified Polytropic Equation of State

Ilona Bednarek [1], Wiesław Olchawa [2], Jan Sładkowski [1,*] and Jacek Syska [1]

[1] Institute of Physics, University of Silesia, 75 Pułku Piechoty 1, 41-500 Chorzów, Poland
[2] Institute of Physics, University of Opole, Oleska 48, 45-052 Opole, Poland
* Correspondence: jan.sladkowski@us.edu.pl; Tel.: +48-323493892

Abstract

The nuclear symmetry energy is a key component of the equation of state of neutron stars, controlling their macroscopic parameters and internal structure. Currently, it remains an unknown issue in both experimental and theoretical studies within the density range relevant to the interiors of neutron stars. This paper aims to investigate the density dependence of the symmetry energy, analyzing it in terms of the curvature parameter K_{sym}. The analysis is based on a neutron star matter equation of state constructed using the proposed modified polytropic form. The used polytropic equations of state approximate the complex, realistic ones. The realistic equations of state selected for the analysis in this paper are those derived using the relativistic mean-field approach. The proposed method exploits the existing strong correlations between the incompressibility of both symmetric and asymmetric nuclear matter and the calculated values of the neutron star crust-core transition density. Starting from the experimental constraint on the incompressibility of symmetric nuclear matter K_0 and based on observationally determined parameters, such as the mass and radius of PSR J0740+6620 pulsar, the formulated method allows for a selection of the range of K_{sym} values acceptable by both the constraints on K_0 and the results of astrophysical observations.

Keywords: symmetry energy; polytropic equation of state; neutron stars

---

1. Introduction

The complexity of high-density, high-isospin-asymmetry systems is why correctly describing the properties of nuclear matter remains a significant challenge in both nuclear physics and astrophysics. Thus, determining the properties of such systems, which are mainly represented by neutron stars, necessitates the use of different methods in the employed analysis. The starting point for such an analysis is the equation of state for neutron star matter. Generally speaking, an equation of state is a thermodynamic formula that describes the properties of matter under given physical conditions. Since neutron star matter has extremely unique properties, knowledge of its equation of state remains limited, especially regarding the density in its interior, which can reach values several times the saturation density n_0. The search continues for an equation of state that accurately describes matter over the density and pressure ranges relevant to neutron stars. The current state of astrophysical observation is sufficiently advanced to place constraints on the equation of state of dense nuclear matter, thereby justifying the selection of a model from a vast number of theoretical models. Thus, astrophysical observations have entered into a complementary relationship with nuclear theory, providing constraints on the equation of state of nuclear matter at densities and isospin asymmetries beyond those accessible in ground-based experiments. The essential observable parameters of a neutron star are its mass, radius, moment of inertia, and tidal deformability. The structure equations for spherically symmetric relativistic stars in hydrostatic equilibrium - the Tolman - Oppenheimer - Volkoff (TOV) equation supplemented by an equation of state, relate macroscopic, measurable neutron star properties with the properties of neutron star matter. The simplest neutron star model considers only neutrons, protons, and leptons, as well as their effective interactions. However, as our understanding of the neutron star structure deepens, it has become clear that its chemical composition does not necessarily consist solely of nucleons. With this in mind, more advanced models of neutron stars are being constructed, including, for example, hyperons and quarks. A critical parameter for verifying the neutron star equation of state is its mass. For a given equation of state, which makes it possible to model a neutron star, it is necessary to obtain a maximum mass value no smaller than the values obtained from observations. Otherwise, the equation of state is invalid. Accurate measurements of the masses of neutron stars place their value at approximately $2M_{\odot}$, indicating that the equation of state is relatively stiff. The observations that led to the estimation of neutron star gravitational masses concern PSR J1614-2230 with $M = 1.908^{+0.016}_{-0.016}M_{\odot}$ [1–4] PSR J0348+0432 with $M = 2.01 \pm 0.04M_{\odot}$ [5] and PSR J0740+6620 with an updated value of mass $M = 2.08 \pm 0.07M_{\odot}$ [6,7]. The measured values of pulsar masses, supplemented by upper limits on tidal deformability from gravitational-wave observations, impose even more stringent constraints on equation-of-state models. More information, which will undoubtedly help resolve the issue of an acceptable equation of state of neutron star matter, can be obtained from simultaneous measurements of neutron star radii and masses. NICER [8] measurements of the modulation of the thermal X-ray pulses of rotation-powered millisecond pulsars provide data that enables one to obtain such constraints. Findings from the analyses of NICER observations of PSR J0437–4715, PSR J0030+0451, PSR J1231–1411, PSR J0740+6620 allowed to derive constraints on their masses and radii [9–16]. The results indicate that neutron stars are generally more compact, favoring theoretical models with stiffer equations of state. Gravitational wave detection data provide a complementary approach to constraining the equation of state. Combining multi-mesh observations of the neutron star merger in the binary system GW170817 allows one to determine the radius and mass of the neutron star. Additionally, the gravitational wave signals encode the tidal effects of neutron stars. The result reported by the LiGO and Virgo collaborations, measured at $1.4M_{\odot}$, places it within the range $\Lambda_{1.4} = 190^{+390}_{-120}$ [17,18]. In general, reconstructing physically realistic equations of state is a very complex task. The parameters in the polytropic equations of state are adjusted to reproduce the observational data as closely as possible, thereby creating approximate representations of the physical equation of state. Polytropic models of neutron stars have evolved significantly. They have often been used to approximate the high-density, high-pressure portions of the equation of state. Because these conditions also determine the physical properties of the corresponding realistic, complex equations of state, understanding polytropic models translates into a correct interpretation of realistic equations of state. Several attempts have been made to approximate the equation of state using polytropes. Read et al. [19], following the work of Vuille and Ipser [20], introduced a formalism in which the high-density region was divided into three intervals. In each interval, the polytropic form was used separately to describe the pressure-mass density relationship. This approach resulted in a four-parameter piecewise polytropic fit that was more accurate at reproducing the equation of state of realistic models. This approximation to the equation of state enables accurate predictions of neutron star observables, including mass, radius, and moment of inertia. A drawback of this approach is the discontinuity of the sound velocity.

Another formalism for modeling the neutron star equation of state was introduced by Lindblom [21]. This method uses mathematical series to obtain a good match between pressure and energy density. This type of parametric representation, being constructed from a generating function expressed as a linear combination of fixed basis functions, e.g., polynomial or trigonometric functions, achieves very high accuracy in reproducing realistic equations of state. In this paper, an alternative form of the polytrope formalism that accurately reproduces the observationally determined mass and radius of a neutron star is developed. For the analysis carried out in this paper, the pulsar PSR J0740+6620 was selected. The applied approach yields algebraically simple formulas that can be easily implemented for subsequent calculations. Using experimental constraints on the symmetric nuclear matter incompressibility K_0, a correlation and linear regression analysis was performed between K_0 and neutron star crust-core transition density n_{bt}. Based on the presented modified polytropic equation of state, for the determined range of n_{bt} values, and for the remaining polytropic parameters adjusted to reproduce mass and radius values consistent with astrophysical observations of the PSR J0740+6620 pulsar, a correlation and linear regression analysis was then performed between n_{bt} and the symmetry energy curvature parameter K_{sym}, allowing for the estimation of the range of K_{sym} values favored by the observed pulsar mass and radius. A description of the procedure and the results of the analysis are presented in the section Results and in Appendix A.3.

2. Parameterization of the Equation of State

2.1. Polytropic Forms of the Equation of State

The entire analysis presented in this paper is based on a modification of the well-known polytropic form of the equation of state provided by the formula

$$P(\rho) = K\rho^{\Gamma}, \tag{1}$$

where K is the polytropic constant, ρ denotes the density of matter. More generally, the adiabatic index $\Gamma(P)$ written as

$$\Gamma(P) = \frac{n_b}{P}\frac{dP}{dn_b} = \frac{\varepsilon + P}{P}\frac{dP}{d\varepsilon}, \tag{2}$$

is a parameter that, at a given density, characterizes the stiffness of the equation of state, n_b denotes the baryon number density, $\varepsilon = \rho c^2$ is the energy density of the system. For a given $\Gamma(P)$, the equation of state considered as a function $\varepsilon(P)$ is calculated by integrating this first-order ordinary differential equation

$$\frac{d\varepsilon(P)}{dP} = \frac{\varepsilon(P) + P}{P\Gamma(P)}. \tag{3}$$

The pressure can be calculated based on thermodynamic considerations from the following relationship

$$P(n_b) = n_b^2 \frac{d}{dn_b}\left(\frac{\varepsilon(n_b)}{n_b}\right) = n_b \frac{d\varepsilon(n_b)}{dn_b} - \varepsilon(n_b). \tag{4}$$

Using the chain rule, equations (3) and (4) can be written as:

$$\frac{dP(n_b)}{dn_b} = \frac{P(n_b)\Gamma(p(n_b))}{n_b}. \tag{5}$$

The calculations performed are based on a detailed analysis of a pair of differential equations, where the equation of state $\varepsilon(P)$ is a solution of the differential equation (3), and the pressure dependence on n_b is governed by the differential equation (5). In general, there are several approaches to solving the equation of state (3). Using the formalism introduced by Vuille and Ipser [20], Read et al. [19] employed an approach that divides the relevant density range into three distinct intervals. In each interval, a polytropic form of the equation of state is applied, and for each density interval, the corresponding values of K and Γ are determined. This approach yields a four-parameter approximate model, commonly known as a piecewise polytropic model. An alternative model was presented by Lindblom in the paper [21], in which a power-law expansion of the adiabatic index $\Gamma(P)$ was proposed. This allows obtaining the equation of state $\varepsilon(P)$ from the solution of the differential equation (3) by inserting the appropriate spectral representation of $\Gamma(P)$.

Analyzing Eq.(3) and (5), it is evident that the parameter $\Gamma(P)$ in both equations appears in the product $P\,\Gamma(P)$. Thus, it is particularly informative to examine the dependence of quantity $P\Gamma(P)$ on pressure P. This was done by relating the analyzed polytropic equations of state to more realistic ones for neutron stars. In the performed analysis, the relativistic mean-field (RMF) model class has been chosen. Their construction uses a field-theoretic framework, in which nucleon-nucleon interactions are modeled through meson exchange. The applied relativistic mean-field (RMF) models incorporate various nonlinear mixed meson terms, which enhance these models' ability to provide satisfactory descriptions of the properties of asymmetric nuclear matter.

In a vast majority of RMF models, when the pressure is sufficiently large, the product $P\Gamma(P)$, considered as a function of P, can be approximated by a linear relationship of the form:

$$P\Gamma(P) = \gamma_0(P + P_0), \tag{6}$$

where γ_0 and P_0 are parameters chosen in the approximation procedure. Therefore, in this approximation $\Gamma(P)$ can be written as follows:

$$\Gamma(P) = \gamma_0\left(1 + \frac{P_0}{P}\right). \tag{7}$$

Inserting the above expression into the differential equations (5) and (3), one can obtain exact solutions and write them in the following form:

$$P(n_b) = -P_0 + Kn_b^{\gamma_0}, \tag{8}$$

$$\varepsilon(n_b) = P_0 + (1 + a)M_{\rm nuc}n_b + \frac{K}{\gamma_0 - 1}n_b^{\gamma_0}, \tag{9}$$

where $M_{\rm nuc}$ is the nucleon mass, and K and a are appropriately chosen (see below) integration constants. Note that if $P_0 = 0$ in Eq. (8) and (9), these expressions become identical to the ones that define the piecewise polytropic equation of state for a sequence of density intervals [19]. The obtained formulas (8) and (9) refer only to the description of the stellar core, while the analytical representation presented in Table II of [19] has been used to describe the stellar crust. At the core-crust boundary it has been assumed that both the energy density and the pressure are continuous, i.e. $\varepsilon_{\rm core}(n_{bt}) = \varepsilon_{\rm crust}(n_{bt})$ and $P_{\rm core}(n_{bt}) = P_{\rm crust}(n_{bt})$, where n_{bt} denotes the baryon number density n_b at the core-crust boundary. Therefore, for the fixed value of n_{bt}, $\varepsilon_{\rm crust}(n_{bt})$ and $P_{\rm crust}(n_{bt})$ are also known. Thus, assuming the continuity of these physical quantities, the constants of integration can be found:

$$K = (P_t + P_0)/n_{bt}^{\gamma_0}, \tag{10}$$

$$a = \frac{(\gamma_0 - 1)\varepsilon_t - P_t - P_0\gamma_0}{(\gamma_0 - 1)M_{\rm nuc}n_{bt}} - 1, \tag{11}$$

where $\varepsilon_t \equiv \varepsilon_{\rm crust}(n_{bt})$ oraz $P_t \equiv P_{\rm crust}(n_{bt})$.

If the product $P\Gamma(P)$ can be approximated by Eq. (6), then the method applied to represent the equation of state using the shifted by $-P_0$ polytropic form given by Eq. (8) is valid. This asymptotic approximation more reasonably represents the course of $P\Gamma(P)$ in the high-pressure limit. This was verified by analyzing the behavior of $P\Gamma$ as a function of P for selected realistic equations of state. Figure 1 shows the chosen equations of state given in terms of $P(n_b)$ dependence and the $P\Gamma(P)$ dependence on P for selected equations of state of the RMF models. In most cases, one can distinguish a linear part of the function $P\Gamma(P)$. For a given equation of state from the RMF group of models, the corresponding one represented by the shifted polytropic equation of state is also presented for comparison. Dashed lines indicate the modified polytropic equations of state. The inset in this figure represents the analyzed quantity $P\Gamma(P)$ as a function of pressure P. It is apparent that among the various RMF models, there are some for which the linear approximation of $P\Gamma(P)$ is reliable for a wide range of pressures. By the equation of state corresponding to a given polytropic equation, the equation of state calculated based on the RMF model, characterized by the same value of the crust-core transition density n_{bt}, is meant. The remaining parameters of the polytropic model were adjusted to obtain a maximum mass close to the value of the corresponding RMF model. By comparing the equations of state for each case of the RMF model with the corresponding modified polytropic approximations, one can determine a common pressure range of the order of $[80\,\mathrm{MeVfm^{-3}}, 600\,\mathrm{MeVfm^{-3}}]$, for which the applied approximation best reproduces the realistic equation of state. Having obtained the equation of state, the stellar structure can be modeled using the Tolman-Oppenheimer-Volkoff (TOV) equation. Solutions of the structure equations show that this pressure range corresponds to the maximum mass configuration of the given equation of state. Thus, the applied linear approximation to the $P\Gamma(P)$ function and the resulting form of the shifted polytropic equation of state well reproduce the structure of a maximum mass star. Therefore, the analysis conducted in this paper focused on the maximum-mass configuration for the given equations of state. The number of parameters required to achieve a reasonable level of accuracy in fitting the polytropic form of the equation of state to the corresponding neutron star equations of state has been reduced to three in this case. The calculations have been performed based on the parameters of the RMF models analyzed in [22–24]. Here, the individual equations of state follow the abbreviations used in those papers.

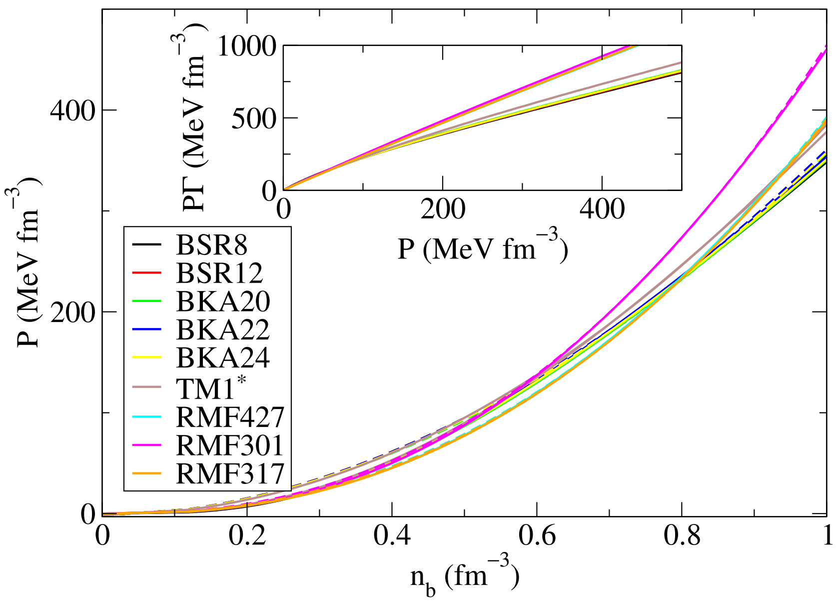

Figure 1. The equations of state given in terms of $P(n_b)$ dependence. These equations were obtained for the selected group of RMF models. The dashed lines represent the fitted polytropic equations of state, colored to match the corresponding RMF models. The inset presents the product $P\,\Gamma(P)$ as the function of P calculated for the same group of models.

2.2. Taylor Expansion

The commonly used method for describing the nuclear matter equation of state is parameterization, which uses empirical coefficients directly linked to nuclear matter's properties. In general, the function which represents an equation of state of nuclear matter considered as its binding energy per nucleon $E(n_b, \delta_a)$, depends on the baryon number density $n_b = n_n + n_p$, where n_n and n_p are neutron and proton number densities, and the isospin asymmetry parameter $\delta_a = (n_n - n_p)/(n_b)$. The function $E(n_b, \delta_a)$ can be approximated by a partial sum of terms of its Taylor series. The expansion around the point of zero isospin asymmetry $\delta_a = 0$ partitions the nuclear system into the symmetric and asymmetric components

$$\begin{aligned} E(n_b, \delta_a) &= E(n_b, \delta_a = 0) + \frac{1}{2}\frac{\partial^2 E(n_b, \delta_a)}{\partial \delta_a^2}|_{\delta_a=0}\delta_a^2 + \ldots \\ &= E_0(n_b) + E_{sym,2}(n_b)\delta_a^2 + \ldots, \end{aligned} \tag{12}$$

where $E(n_b, \delta_a = 0) \equiv E_0(n_b)$ is the binding energy of the symmetric matter. The asymmetric part defines the symmetry energy $E_{sym,2}(n_b)$, in the case when the expansion given by Eq. (12) is restricted to the second-order term only. The symmetry energy, considered as the energy difference between pure neutron matter (PNM) $E_{PNM}(n_b) = E(n_b, \delta_a = 1)$ and symmetric matter (SNM) $E_{SNM}(n_b) \equiv E_0(n_b)$ can be written as

$$E_{sym}(n_b) = E_{PNM}(n_b) - E_{SNM}(n_b). \tag{13}$$

The function $E_{sym}(n_b)$ can be represented by expanding it in a Taylor series around the saturation density n_0, which allows defining the expansion coefficients

$$E_{sym}(n_b) = E_{sym}(n_0) + L\left(\frac{n_b - n_0}{3n_0}\right) + \frac{1}{2}K_{sym}\left(\frac{n_b - n_0}{3n_0}\right)^2 + \ldots, \tag{14}$$

The main coefficients that characterize the dependence of the symmetry energy on density are $E_{sym}(n_0)$ being the symmetry energy parameter at n_0, the symmetry energy slope $L = 3n_0 \frac{dE_{sym}(n_b)}{dn_b}|_{n_0}$, and curvature $K_{sym} = 9n_0^2 \frac{d^2E_{sym}(n_b)}{dn_b^2}|_{n_0}$. Subsequently, the Taylor series expansions at the saturation density n_0 of the symmetric $E_0(n_b)$ part approximate this function by the following formula:

$$E_0(n_b) = E_0(n_0) + \frac{K_0}{2}\left(\frac{n_b - n_0}{3n_0}\right)^2 + \ldots, \tag{15}$$

In the case of symmetric matter, the key coefficients are the symmetric matter binding energy at saturation density $E_0(n_0)$ and the incompressibility parameter $K_0 = 9n_0^2 \frac{d^2E_0(n_b)}{dn_b^2}|_{n_0}$.

The coefficients of the expansion (14) characterize the properties of isospin asymmetric nuclear matter. Neutron star matter possesses a very high excess of neutrons over protons, and therefore a high value of isospin asymmetry. Consequently, it is expected that information about the symmetry energy $E_{sym}(n_b)$ is encoded in the properties of neutron stars. One of the most essential characteristics of the internal structure of neutron stars is the stratification of matter inside them. The primary challenge in determining it is identifying the transition density between the crust and the neutron star core. Its correct location allows one to estimate the crust's physical properties, such as thickness, mass fraction, and moment of inertia. Since there is a relationship between the parameter δ_a and the relative proton concentration $\delta_a = 1 - 2Y_p$, where $Y_p = n_p/n_b$, the binding energy $E(n_b, \delta_a)$ can also be written as a function of the proton concentration $E(n_b, Y_p)$. There are various approaches to determining the transition density n_{bt}. One of these is based on the condition of thermodynamic stability of n-p-e matter with respect to the growth of small density fluctuations. Details on how to determine the transition density can be found, for example, in the following papers [25,26]. Having obtained the value of the transition density n_{bt}, it is possible to determine the properties of matter in the vicinity of this point, such as the equilibrium concentration of protons, pressure, and energy density.

The next step in the analysis is to determine the correlation between the transition density n_{bt} and the properties of nuclear matter. To ensure the reliability and interpretability of the obtained results, it is essential to consider existing experimental constraints on the most important properties of this matter. Experimental constraints obtained for symmetric nuclear matter ($\delta_a = 0$) mainly concern its incompressibility K_0 at the saturation density. The estimated value of K_0 is in the range 230 ± 20 MeV [27–29]. In the case of asymmetric nuclear matter, experimental constraints concern key coefficients that characterize the density dependence of the symmetry energy. The collected results of 23 analyses performed before 2013 supplemented with the results of 59 analyses in 2016 allowed for the following estimates of the symmetry energy value at the saturation density $E_{sym,2}(n_0)$ [30]: $E_{sym}(n_0) = 31.6 \pm 2.7$ MeV [31] and $E_{sym}(n_0) = 31.7 \pm 3.2$ MeV [32], and for the symmetry energy slope the values $L = 58.9 \pm 16$ MeV [31] and $L = 58.7 \pm 28.1$ MeV [32]. Results obtained from neutron star observations yield an average value of $L = 57.7 \pm 19$ MeV. The constraints on the symmetry energy curvature K_{sym} [30] resulted from the analysis presented by Mondal et al. [33], giving the value of $K_{sym} \approx -112 \pm 71$ MeV, whereas the finding by Margueron et al. [34] gives $K_{sym} \approx -100 \pm 100$ MeV. The average value of the curvature of the symmetry energy K_{sym} inferred from analyses of neutron star observations since GW170817 is $K_{sym} \approx -107 \pm 88$ MeV [30].

3. Results

The modified polytropic equation of state, employed in the performed analysis, for the chosen group of parameters (n_{bt}, γ_0, P_0), satisfies the causality condition (the sound velocity $v_s < c$). The analysis focused on developing a modified polytropic equation of state. Having specified such an equation of state, the stellar structure equations can be solved. This enables the construction of neutron star models that not only satisfy key astrophysical constraints but also facilitate the discovery of relationships between neutron star macroscopic parameters and the selected properties of nuclear matter. The approximate form of the equation of state was tested against a selected group of RMF models, which, in addition to satisfying constraints on the properties of nuclear matter, were also characterized by a sufficiently large maximum mass. The results of the analysis concern the change in the value of the maximum mass configuration, M_{max}, and its radius, for which the notation R_{max} is adopted. The allowable changes in both quantities are within the limits set by the observational data for the pulsar PSR J0740 6640. For the mass they are given by $M_{max} = 2.073 \pm 0.069\, M_{\odot}$, thus $M_{lower} = 2.006\, M_{\odot}$ and $M_{upper} = 2.139\, M_{\odot}$. For the radius $R_{max} = 12.55^{+1.28}_{-0.88}$ km, thus $R_{upper} = 13.69$ km and $R_{lower} = 11.41$ km.

A characteristic feature of the calculated modified polytropic equations of state was that they reproduced maximum masses within the range [M_{lower}; M_{upper}]. The transition density value for these models was chosen to be consistent with the n_{bt} values determined for the RMF models.

Applying the linear approximation given by Eq. 6 to the function representing the product $P\,\Gamma(P)$, the modified polytropic model yields analytical solutions for the energy density and pressure. Having obtained the modified polytropic model, it was subsequently used to establish a relationship with the Taylor expansion parametrized model, which depends on the properties of nuclear matter. For this purpose, a procedure was developed that exploits existing correlations between parameters characterizing nuclear matter and the density n_{bt} at the neutron star crust-core boundary. The analysis of correlations carried out for the RMF group of models showed that the strongest correlations occur between n_{bt} and symmetric nuclear matter incompressibility K_0, as well as between n_{bt} and incompressibility of the asymmetric nuclear matter K_{sym}. Two linear regression functions n_{bt} (fm^{-3}) vs. K_0 (MeV) and K_{sym} (MeV) vs. n_{bt} (fm^{-3}) were obtained,

$$\widehat{n_{bt}} = 0.0066 + 0.00027\, K_0 \tag{16}$$

and

$$\widehat{K_{\mathrm{sym}}} = 347.917 - 5181.025\, n_{bt}\ , \tag{17}$$

where $\widehat{n_{bt}}$ and $\widehat{K_{\mathrm{sym}}}$ are the theoretical means of the density n_{bt} and K_{sym}, respectively. The analysis was conducted on the sample of $N = 24$ RMF models. The numerical details of the regression analysis are provided in the Appendix, along with basic information on the univariate regression. Since the incompressibility of symmetric nuclear matter K_0 is considered to be one of the most essential experimental constraints, the existing strong correlation between n_{bt} and K_0 was used to estimate the range of n_{bt} consistent with experimentally acceptable K_0 values. Based on the obtained regression equation (16), the n_{bt} values corresponding to the upper and lower bounds of the experimental constraints on K_0 were estimated. These boundary values of the transition density are 0.05876 fm^{-3} and 0.07527 fm^{-3} respectively. The next step in the procedure was to determine the remaining two parameters, γ_0 and P_0, of the modified polytropic equation of state for both n_{bt} boundary values. In Figure 2, two regions of the (γ_0, P_0) parameter space are presented. The region marked cyan corresponds to the fixed value of $n_{bt} = 0.05876$ fm^{-3}, for the region in gray the fixed value of n_{bt} equals 0.07527 fm^{-3}. The individual region encompasses the set of possible parameters γ_0 and P_0 that, for a given value of n_{bt}, are adjusted to account for the observational constraints on the mass and radius of the pulsar PSR J0740+6620. The results of the performed analysis presented in Figure 2 illustrate the change in the value of the maximum mass configuration M_{max} and its radius. For the obtained boundary values of n_{bt}, the curves bounding the individual regions (iso-indicial contours with masses) represent the set of parameters γ_0 and P_0 that allow for obtaining models of stars with a constant mass equals M_{lower}=2.006 $M_\odot$ — parts of curves A_1B_1 and A_2B_2, and stars with a mass of M_{upper}=2.139 $M_\odot$ — curves C_1D_1 and C_2D_2. The sets of parameters γ_0 and P_0 for models of stars with a constant radius are edges A_1C_1 and A_2C_2, with R_{lower} = 11.41 km, and B_1D_1 and B_2D_2, with R_{upper} = 13.69 km. The radius increases from the lower value R_{lower} to the upper value R_{upper} along the iso-indicial curve from A_i to B_i, $i = 1, 2$, while mass increases from 2.006 $M_\odot$ to 2.139 $M_\odot$ between points A_i and C_i, $i = 1, 2$. Points within both regions yield configurations of stars with intermediate values of mass and radius. Still, their values are always within the range of values accepted by the observational results.

Figure 3 and Table 1 present an analysis of the maximum mass variation for the equations of state determined for the parameters γ_0 and P_0 as they vary along the curves bounding the individual regions shown in Figure 2. The dashed lines indicate the observationally obtained constraints on the mass of the pulsar PSR J0740+6620. The lower line corresponds to the mass M_{lower}, while the upper line corresponds to the mass M_{upper}. The separate paths, namely A_1E_1, depict the increase in mass from M_{lower} to M_{upper} with a simultaneous decrease in the n_{bt} from its boundary value 0.05876 fm^{-3} to 0.05367 fm^{-3}, D_1F_1, the decrease in mass value from M_{upper} value to M_{lower} associated with an increase in n_{bt} from 0.05876 to 0.06311 fm^{-3}. Path A_2E_2 represents the increase in mass from the lower value to the upper one with a decrease in the n_{bt} value from the boundary value 0.07527 fm^{-3} to 0.06919 fm^{-3}. The curve D_2F_2 represents the decrease in the mass value from the upper value to the lower value with an increase in n_{bt}. The value of n_{bt} for the point F_2 is 0.08056 fm^{-3} The n_{bt} boundary values of 0.05876 fm^{-3} and 0.07527 fm^{-3}, respectively, were obtained based on the regression equation (16). The n_{bt} values for points E_1, F_1, E_2, and F_2 were determined for the range of parameters γ_0 and P_0 obtained using observational constraints on the mass and radius of the PSR J0740 6640 pulsar. Thus, at this stage of the analysis, the value of n_{bt} varies from the boundary values determined by the regression equation (16) to the ones that are consistent with observational constraints on the pulsar's mass and radius. This yields an updated range of n_{bt} values from 0.055367 fm^{-3} to 0.08056 fm^{-3}. Then, the regression equation given by (17) made it possible to estimate the range of K_{sym} corresponding to the values of n_{bt} from the range [0.055367 fm^{-3}; 0.08056 fm^{-3}]. The interpretation of points E_1, F_1, E_2, and F_2 is presented in Figure 4 and Table 1.

Figure 4 and Table 1 illustrate the change in the radius of the maximum mass configuration resulting from the change in the value of n_{bt} within the updated range [0.055367 fm^{-3}; 0.08056 fm^{-3}]. The parameters γ_0 and P_0 belong to the bounding curves of the individual regions presented in Figure 2. In all figures, points labeled in the same way have the same coordinates, as given in Table 1. The path A_1E_1, corresponding to the increase in mass from M_{lower} to M_{upper} value, reaches a radius of 12.14 km at point E_1. This value is smaller than the radius R_{upper}. Still, it cannot be increased because it would result in a stellar configuration with a mass exceeding its upper limit M_{upper} inferred from observations. Similar radius constraints were obtained for the remaining points. Points F_1 and F_2 correspond to stars with the mass equal to M_{lower} but radii larger than the R_{lower} values. Point E_2, like point E_1, represents a star with the mass value M_{upper} and the radius smaller than the R_{upper} value. Although the correlations n_{bt} vs. K_0 and K_{sym} vs. n_{bt} are strong, they are not perfect. Therefore, a direct conversion of the constraint from K_0 to K_{sym} by eliminating n_{bt} from the regression equations cannot be applied. The direct correlation between K_{sym} and K_0 is moderately negative. Meanwhile, having specified the updated range of the transition density n_{bt} and using the regression equation (17) enables one to specify the range of K_{sym} that is favored by both the experimental constraints on K_0 and the pulsar observations. The analysis indicates a range of K_{sym} values of [-69.5 MeV, 70 MeV], in agreement with other experimental constraints.

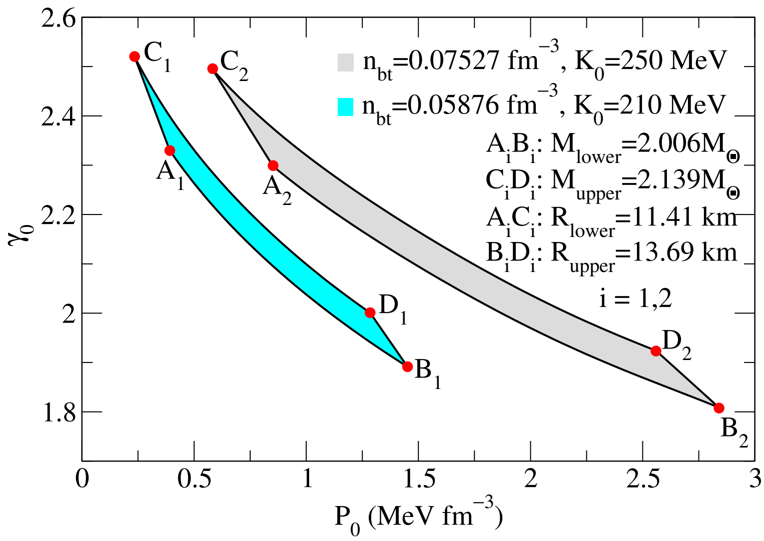

Figure 2. Two selected regions of parameters that contain sets of pairs (γ_0, P_0). The region in cyan contains points with coordinates (γ_0, P_0), which for the density value of $n_{bt} = 0.05876$ fm^{-3} yield the maximum mass models with mass and radius values within the ranges (M_{lower}, M_{upper}) and (R_{lower}, R_{upper}). The gray region is a similar set of points, differing in the value of $n_{bt} = 0.07527$ fm^{-3}. The sets of parameters (γ_0, P_0) corresponding to the curves that bound the individual regions lead to configurations of stars with constant masses equal to M_{lower} for A_1B_1 and A_2B_2, and M_{upper} for C_1D_1 and C_2D_2, respectively. The sets of parameters (γ_0, P_0) that give models of stars with constant radii equal to R_{lower} are the edges of A_1C_1 and A_2C_2, while those with constant radii equal to R_{upper} are the edges of B_1D_1 and B_2D_2. Points within both regions yield configurations of stars with mass and radius values within the range of values determined by observations.

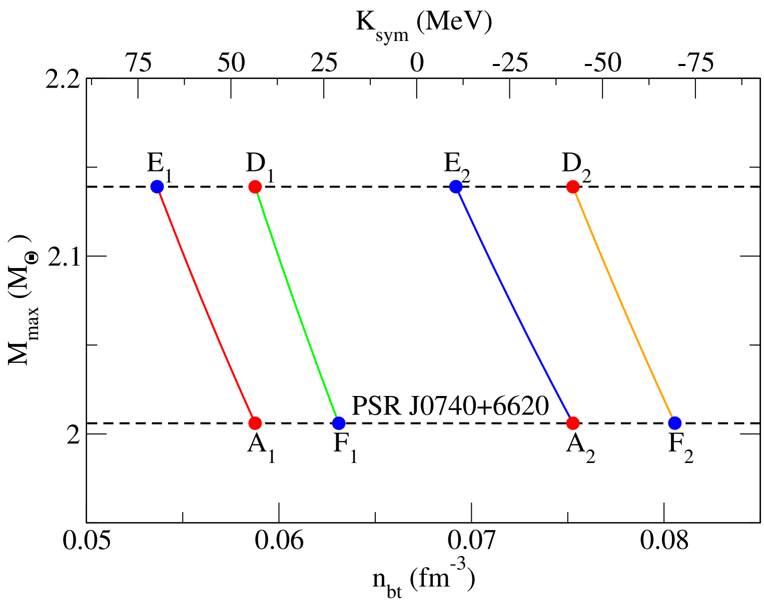

Figure 3. The points are characterized by values of the parameters γ_0 and P_0 consistent with those in Figure 2. For points A_1 and D_1, the value of n_{bt} is equal to 0.05876 fm^{-3}, while for points A_2 and D_2, $n_{bt} = 0.07527$ fm^{-3}. The change in the value of the maximum mass is caused by a change in the value of the third parameter – the transition density n_{bt}. In the case of point A_1, the mass increases from M_{lower} to M_{upper}, which is reached at point E_1 for a value of n_{bt} equal to 0.05367 fm^{-3}. At point D_1, the maximum mass decreases from M_{upper}, reaching point F_1 for a density of $n_{bt} = 0.06311$ fm^{-3}. Then the maximum mass equals M_{lower}. A similar analysis was performed for points A_2, with a transition to point E_2, and D_2, with a transition to point F_2. The exact coordinate values of these points are presented in Table 1. The horizontal axes show n_{bt} and K_{sym}. The scale for K_{sym} was determined based on the regression equation (17).

 doi:10.20944/preprints202602.0114.v1

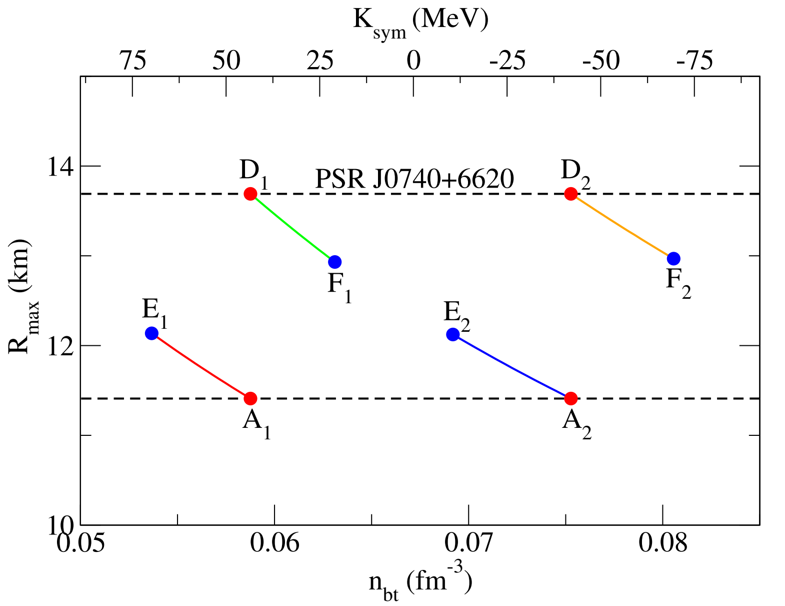

Figure 4. The change in radius of the maximum-mass configuration R_{max} that corresponds to the mass changes shown in Figure 3. Point E_1 corresponds to the maximum radius that a star with a maximum mass equal to M_{upper} can reach when the value of n_{bt} decreases from 0.05876 fm^{-3} to 0.05367 fm^{-3}. Similarly, for point D_1, the mass decreases from M_{upper} to M_{lower}, and n_{bt} increases from 0.05876 fm^{-3} to 0.06311 fm^{-3}. At point F_1, where the mass is equal to M_{upper}, the radius reaches the value 12.93 km. A similar analysis was performed for points marked with index 2. Data on the radii and n_{bt} density appear in Table 1. The dashed lines represent the obtained constraints on the PSR J0740+6620 radius. On the horizontal axis, there are the transition density n_{bt} and K_{sym} parameter determined based on the regression equation (17).

Table 1. The data corresponding to points shown in Figures 2–4. The limits of permissible changes in the mass and radius of the modeled neutron star adopted in this paper are: $M_{lower} = 2.006M_{\odot}$, $M_{upper} = 2.139M_{\odot}$, $R_{lower} = 11.41$ km, $R_{upper} = 13.69$ km.

Point	n_{bt} (fm^{-3})	P_0 (MeV fm^{-3})	γ_0	M_{max} $M_{\odot}$	R (km)
A_1		0.3918	2.330	M_{lower}	R_{lower}
B_1	0.05876	1.452	1.891	M_{lower}	R_{upper}
C_1		0.2350	2.520	M_{upper}	R_{lower}
D_1		1.285	2.001	M_{upper}	R_{upper}
E_1	0.05367	0.3918	2.330	M_{upper}	12.14
F_1	0.06311	1.285	2.001	M_{lower}	12.93
A_2		0.8523	2.299	M_{lower}	R_{lower}
B_2	0.07527	2.841	1.808	M_{lower}	R_{upper}
C_2		0.5831	2.496	M_{upper}	R_{lower}
D_2		2.559	1.923	M_{upper}	R_{upper}
E_2	0.06919	0.8523	2.299	M_{upper}	12.12
F_2	0.08056	2.559	1.923	M_{lower}	12.97

4. Discussion

The modified polytropic model is a simplified version of the equation-of-state parameterization, characterized by fewer parameters. It requires only three parameters: γ_0, P_0, and the crust-core transition density n_{bt}. The fact that the model contains only three parameters is undoubtedly an advantage, as it allows easy control over their changes relative to the neutron star's physical parameters. The exploited initial range of the crust-core transition density n_{bt} was obtained using regression analysis of n_{bt} vs. K_0, considering current experimental constraints on K_0. The established n_{bt} range was then used, together with the observational constraints on the mass and radius of pulsar PSR J0740+6620, to determine a

 doi:10.20944/preprints202602.0114.v1

two-dimensional region of parameters P_0 and γ_0. The obtained parameters of the equation of state are of two types: n_{bt} was determined based on the properties of nuclear matter, while γ_0 and P_0 were determined based on astrophysical observations. The determined ranges of γ_0 and P_0 were then used to find a relationship between n_{bt} and K_{sym}. For these ranges of P_0 and γ_0, the updated range of n_{bt} compared to the initial one was obtained. Then, after performing the regression K_{sym} vs. n_{bt}, bounds on K_{sym} were established from the updated range of n_{bt}. As a result of the applied procedure, the boundary values of n_{bt} for points E_1 and F_2 were shifted towards lower values in comparison to the ones from the RMF sample of models (Table A1). This, due to the negative correlation between K_{sym} and n_{bt}, results in a systematic shift of the average theoretical values of K_{sym} towards higher values $-69.47\,\mathrm{MeV} \leq K_{sym}$ $\leq 69.85\,\mathrm{MeV}$, (Table A1). The described method enabled the transition from experimental constraints on K_0 to K_{sym}, which should not be done directly due to the only moderate correlation between K_0 and K_{sym}. The reasons are as follows. The pressure and density values at the crust-core boundary were determined based on thermodynamic relations and depend directly on parameters characterizing nuclear matter, both the symmetric and the isospin-asymmetric parts. Thus, it is reasonable to expect that the correlations between n_{bt} and K_0, and between K_{sym} and n_{bt}, have a physical basis. Therefore, significant correlations between these variables ($r_{K_0\,n_{bt}} = 0.815$ and $r_{n_{bt}\,K_{\rm sym}} = -0.81$) can be used to apply regression functions to determine the practical relationship between them. A similar analysis of the direct transition between K_0 and K_{sym} is unjustified because the physical basis for such a relationship is uncertain.

Author Contributions: Conceptualization, I.B.,W.O., J.Sł. and J.S.; methodology, I.B.,W.O., J.Sł. and J.S.; software, I.B. and W.O.; validation, I.B.,W.O., J.Sł. and J.S.; formal analysis, I.B.,W.O., J.Sł. and J.S.; investigation, I.B.,W.O., J.Sł. and J.S.; writing—original draft preparation, I.B.,W.O., J.Sł. and J.S.; writing—review and editing, I.B.,W.O., J.Sł. and J.S. All authors have read and agreed to the published version of the manuscript.

Funding: This research received no external funding.

Institutional Review Board Statement: Not applicable.

Informed Consent Statement: Not applicable.

Data Availability Statement: No new data were created.

Conflicts of Interest: The authors declare no conflicts of interest

Appendix A

For a sample of N models chosen randomly from a population of models, the linear regression model, $Y_i = \alpha_0 + \alpha_1\, X_i + E_i\,, i = 1, 2, ..., N$, can be estimated by

$$Y_i = \hat{\alpha}_0 + \hat{\alpha}_1\, X_i + \widehat{E}_i\;, \quad i = 1, 2, ..., N\;, \tag{A1}$$

where

$$\widehat{Y}_i := \hat{\alpha}_0 + \hat{\alpha}_1\, X_i \tag{A2}$$

is the conditional (theoretical) mean of Y_i in the $N-$dimensional sample, $\hat{\alpha}_0$, $\hat{\alpha}_1$ are the estimators of the structural parameters α_0, α_1 and $\widehat{E}_i$ is the estimator of the error term E_i. In a given sample, the estimators $\hat{\alpha}_i$ take values that estimate the structural parameters α_i, $i = 0, 1$. The variance of the error term $\widehat{E}_i$ is denoted by MSE (mean squared error). In this paper, for the regression n_{bt} vs. K_0 the response Y is the density n_{bt}, and $\widehat{n_{bt}} \equiv \widehat{Y}$ is its conditional mean. For the regression $K_{\rm sym}$ vs. n_{bt} the response Y is the symmetry parameter K_{sym}, and $\widehat{K_{\rm sym}} \equiv \widehat{Y}$ is its conditional mean.

Appendix A.1. The Linear Correlation Coefficient

The measure of the strength and direction of the linear correlation between two variables X and Y in the population is the Pearson correlation coefficient $R_{XY} \in < -1, +1 >$, [35,36]. For the sake of

Preprints.org (www.preprints.org) | NOT PEER-REVIEWED | Posted: 2 February 2026 doi:10.20944/preprints202602.0114.v1

completeness, the following formulas are given. In a N-dimensional sample, the estimator of R_{XY} is the complete linear correlation coefficient r_{XY} [35,36]:

$$r_{XY} = \frac{cov(X,Y)}{\hat{\sigma}(X)\,\hat{\sigma}(Y)}\,, \tag{A3}$$

where $cov(X,Y)$ is the estimator of the covariance of X and Y (in a sample of size N):

$$cov(X,Y) = \frac{1}{N}\sum_{i=1}^{N}(X_i - \langle X\rangle)(Y_i - \langle Y\rangle)\,, \tag{A4}$$

whereas

$$\hat{\sigma}(X) = \sqrt{\frac{1}{N}\sum_{i=1}^{N}(X_i - \langle X\rangle)^2} \tag{A5}$$

is the estimator of the standard deviation of the variable X and

$$\langle X\rangle = \frac{1}{N}\sum_{i=1}^{N}X_i \tag{A6}$$

is the estimator of its mean value, and the same formulas are used for $\langle Y\rangle$ and $\hat{\sigma}(Y)$.

Appendix A.2. A Regression Function Confidence Band

In the classical normal regression model, the estimator $\widehat{Y}_i = \hat{\alpha}_0 + \hat{\alpha}_1\,X_i$ is the best, unbiased linear (in Y_i) estimator of the conditional expected value $\alpha_0 + \alpha_1\,X_i$, while the estimator of the standard deviation of $\widehat{Y}_i$ has the form [35,36]:

$$\hat{\sigma}(\widehat{Y}_i) = \sqrt{\frac{MSE}{\hat{\sigma}^2(X)\,N}\left(\hat{\sigma}^2(X) + (X_i - \langle X\rangle)^2\right)} \tag{A7}$$

The regression function confidence band for Y_i has therefore the form:

$$\left(\widehat{Y}_i - t(1-\alpha/2,\nu)\,\hat{\sigma}(\widehat{Y}_i), \widehat{Y}_i + t(1-\alpha/2,\nu)\,\hat{\sigma}(\widehat{Y}_i)\right)\,, \tag{A8}$$

where $t(1-\alpha/2,\nu)$ is the $1-\alpha/2$ quantile of the Student's t-distribution with $\nu = N-2$ degrees of freedom. The mean squared error, which appears in Eq.(A7), is in the univariate regression equal to $MSE = SSE/df_{SSE}$, where $SSE = \sum_{i=1}^{N}(Y_i - \widehat{Y}_i)^2$ is called the residual sum of squares (errors) and $df_{SSE} = (N-1)-1$ is the number of degrees of freedom for SSE.

Appendix A.3. The Regression Analysis of n_{bt} vs. K_0 and K_{sym} vs. n_{bt}

The results of linear regression analysis between K_0 and n_{bt}, and n_{bt} and the curvature parameter of the symmetry energy K_{sym} are presented below. The regression functions n_{bt} vs. K_0 and $K_{\rm sym}$ vs. n_{bt} were given in the main text in Eq.(16) and Eq.(17), respectively. The value of the slope coefficients for the regression functions n_{bt} vs. K_0 is equal to $\hat{\alpha}_1 = 0.00027$ fm^{-3} MeV^{-1} (Eq.(16)) and for and $K_{\rm sym}$ vs. n_{bt} is equal to $\hat{\alpha}_1 = -5181.025$ fm^3 MeV (Eq.(17)). Both values are statistically significant. The Pearson correlation coefficients are equal to $r_{K_0\,n_{bt}} = 0.815$ and $r_{n_{bt}\,K_{\rm sym}} = -0.81$ for n_{bt} vs. K_0 and $K_{\rm sym}$ vs. n_{bt}, respectively; thus, both regressions are strong, although not strictly functional. The regression n_{bt} vs. K_0 is positive and $K_{\rm sym}$ vs. n_{bt} is negative. The confidence corridors for both regressions are presented at the 0.99 confidence level. For the regressions, the Kolmogorov-Smirnov normality tests of the residual distribution were performed. There are no grounds to reject the hypothesis of normality of these distributions at the $\alpha = 0.05$ significance level. For n_{bt} vs. K_0, the regression characteristics needed for the calculation of the confidence corridors for the theoretical mean $\widehat{n_{bt}}$, (A2), for which the standard deviation (A7) is needed are, equal to $\langle K_0\rangle = 248.853$, $\hat{\sigma}(K_0) = 22.043$, $MSE = 2.02 \times 10^{-5}$ fm^{-6}. Similarly, for $K_{\rm sym}$ vs. n_{bt}, the results connected with the theoretical mean $\widehat{K_{\rm sym}}$ are as follows: $\langle n_{bt}\rangle = 0.075$, $\hat{\sigma}(n_{bt}) = 0.0074$, $MSE = 845.387$ MeV^2. Additionally, in the considered sample $\langle n_{bt}\rangle = 0.075$, $\langle K_{\rm sym}\rangle = -39.62$ and $\hat{\sigma}(K_{\rm sym}) = 47.444$. The results are illustrated in the following figures.

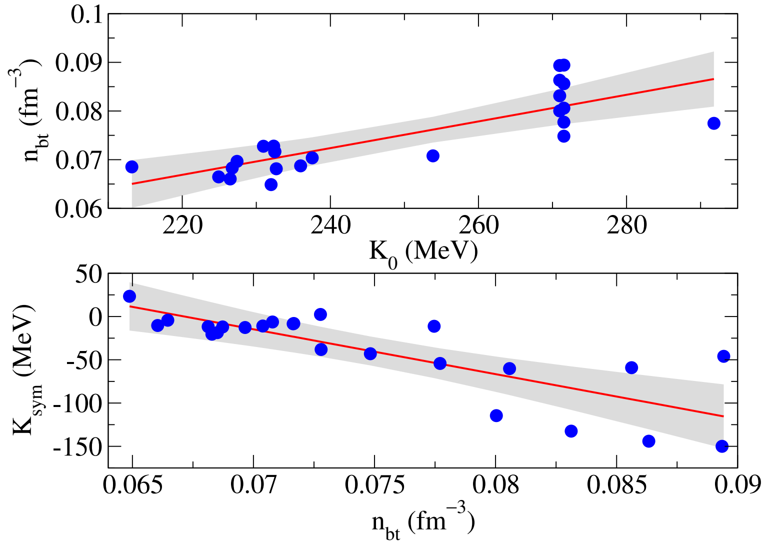

Figure A1. The regression functions n_{bt} vs. K_0 and $K_{\rm sym}$ vs. n_{bt} in the sample of $N = 24$ RMF models and the 99% confidence corridors. The details of the regression analysis for the confidence corridors are given in the text, and the regression functions are given by Eqs. (16) and (17).

Table A1. Values of n_{bt} (fm^{-3}), K_0 (MeV) and $K_{\rm sym}$ (MeV) for the sample of $N = 24$ RMF models and values of the theoretical mean $\widehat{K_{\rm sym}}$, Eq. (17), and the estimator $\hat{\sigma}(\widehat{K_{\rm sym}})$ of the standard deviation of $\widehat{K_{\rm sym}}$, Eq. (A7), for the regression $K_{\rm sym}$ vs. n_{bt} are given. E_1 and F_2 denote the points for the lower and upper limits of the updated range of n_{bt}, respectively.

Model	n_{bt}	K_0	K_{sym}	$\widehat{K_{\rm sym}}$	$\hat{\sigma}(\widehat{K_{\rm sym}})$
E_1	0.0537			69.851	17.923
rmf402	0.0649	231.988	23.371	11.767	9.912
BKA24	0.066	226.476	-10.424	5.747	9.184
BKA22	0.0665	224.915	-4.249	3.591	8.932
rmf317	0.0681	232.696	-11.687	-5.045	7.985
BSR11	0.0683	226.746	-20.421	-5.869	7.9
G2*	0.0685	213.196	-18.679	-7.035	7.782
rmf427	0.0687	235.983	-11.983	-8.144	7.673
BSR10	0.0697	227.394	-12.647	-12.967	7.223
BKA20	0.0704	237.552	-10.929	-16.739	6.908
rmf301	0.0708	253.86	-6.275	-18.822	6.749
FSUGZ03	0.0716	232.471	-8.418	-23.246	6.452
BSR9	0.0717	232.511	-8.095	-23.376	6.444
BSR8	0.0728	230.959	2.363	-29.096	6.154
BSR12	0.0728	232.351	-38.143	-29.236	6.148
NL3v2	0.0748	271.538	-42.95	-39.763	5.935
TM1*	0.0775	291.803	-11.234	-53.426	6.307
NL3v3	0.0777	271.538	-54.196	-54.69	6.375
S271v3	0.08	270.971	-114.5	-66.741	7.265
F_2	0.0806			-69.466	7.516
NL3v4	0.0806	271.538	-60.129	-69.554	7.524
S271v4	0.0831	270.971	-132.463	-82.756	8.924
NL3v5	0.0856	271.538	-59.121	-95.693	10.5
S271v5	0.0863	270.971	-144.112	-99.356	10.972
S271v6	0.0894	270.971	-150.023	-115.033	13.075
NL3v6	0.0894	271.538	-45.944	-115.406	13.126 [1]

Preprints.org (www.preprints.org) | NOT PEER-REVIEWED | Posted: 2 February 2026 doi:10.20944/preprints202602.0114.v1

References

1. Demorest, P.B., Pennucci, T., Ransom, S.M., Roberts, M.S.E., Hessels, J.W.T., Shapiro delay measurement of a 2 solar mass neutron star. *Nature* **2010**, *467*, 1081 – 1083
2. Fonseca, E., Pennucci, T.T., Ellis, J.A. et al., The nanograv nine-year data set: mass and geometric measurements of binary millisecond pulsars. *ApJ*, **2016**, *832*, 167 – 198
3. The NANOGrav 11-year Data Set: High-precision Timing of 45 Millisecond Pulsars. *ApJS*, **2018**, *235*, 37 – 77
4. Agazie, G., Alam, M.F., Anumarlapudi, A. et al., The Nanograv 15-yr Data Set: Evidence for a Gravitational-wave Background. *ApJL*, **2023**, *951*, L8-1 – L8-24
5. J. Antoniadis, P.C.C. Freire, N. Wex, et al., A massive pulsar in a compact relativistic binary. *Science*, **2013**, *340*, 1233232-1 – 1233232-9
6. Cromartie, H.T., Fonseca, E., Ransom, S.M. et al., Relativistic Shapiro delay measurements of an extremely massive millisecond pulsar. *Nature Astronomy*, **2020**, *4*, 72 – 76
7. Fonseca, E., Cromartie, H.T., Pennucci, T.T., et al., Refined Mass and Geometric Measurements of the High-mass PSR J0740+6620. *ApJL*, **2021**, *915*, L12-1 – L12-15
8. Gendreau, K.C., Arzoumanian, Z., Adkins, P.W., et al., The Neutron star Interior Composition Explorer (NICER): design and development. *Proc. SPIE*, **2016**, *9905*, 99051H
9. Miller, M.C., Lamb, F.K., Dittmann, A.J., et al., PSR J0030+0451 mass and radius from NICER data and implications for the properties of neutron star matter. *ApJL*, **2019**, *887*, L24-1 – L24-28
10. T.E. Riley, A.L. Watts, S. Bogdanov, et al., A NICER view of PSR J0030+0451: Millisecond pulsar parameter estimation. *ApJL*, **2019**, *887*, L2-1 – L21-60
11. M.C. Miller, F.K. Lamb,A.J. Dittmann, et al., The Radius of PSR J0740+6620 from NICER and XMM-Newton Data *ApJL*, **2021**, *918*, L28-1 – L28-31
12. T.E. Riley, A.L.Watts, P.S. Ray, et al., A NICER View of the Massive Pulsar PSR J0740+6620 Informed by Radio Timing and XMM-Newton Spectroscopy. *ApJL*, **2021**, *918*, L27-1–L27-30
13. Dittmann, A.J., Miller, M.C., Lamb, F.K., et al., A More Precise Measurement of the Radius of PSR J0740+6620 Using Updated NICER Data. *ApJ*, **2024**, *974*, 295-1 – 295-19
14. Choudhury, D., Salmi, T., Vinciguerra, S., et al., A NICER View of the Nearest and Brightest Millisecond Pulsar: PSR J0437–4715. *ApJL*, **2024**, *971*, L20 -1–L20-38
15. Salmi, T., Deneva, J. S., Ray, P. S., et al., A NICER view of PSR J1231FIX ME!!!!1411: A complex case. *ApJ*, **2024**, *976*, 58-1 – 58-18
16. Salmi, T., Choudhury, D., Kini, Y., et al., The radius of the high-mass pulsar PSR J0740+6620 with 3.6 yr of NICER data. *ApJ*, **2024**, *974*, 294-1 – 294-13
17. Abbott B.P., Abbott, R., Abbott, T.D., Acernese, F., Ackley, K., Adams, C., Adams, T., Addesso, P., Adhikari, R.X. et al. (LIGO Scientific Collaboration and Virgo Collaboration), GW170817: Observation of Gravitational Waves from a Binary Neutron Star Inspiral. *Phys. Rev. Lett.*, **2017**, *119*, 161101-1 – 161101-5
18. Abbott, B.P., Abbott, R., Abbott, T.D., Acernese, F., Ackley, K., Adams, C., Adams, T., Addesso, P., Adhikari, R.X., Adya, V.B., et al. (LIGO Scientific Collaboration and Virgo Collaboration), Properties of the Binary Neutron Star Merger GW170817. *Phys. Rev., X*, **2019**, *9*, 011001-1 – 011001-32
19. Read, J.S., Lackey, B.D., Owen, B.J., Friedman, J.L., Constraints on a phenomenologically parametrized neutron-star equation of state. *Phys. Rev. D* **2009**, *79*, 124032-1 – 124032-18.
20. Vuille, C.; Ipser, J., In *General Relativity and Relativistic Astrophysics*; Eds.; C. P. Burgess and R. C. Myers, American Institute of Physics, College Park Maryland, 1999, *493*, pp. 60 – 62
21. Lindblom, L., Spectral representations of neutron-star equations of state. *Phys. Rev. D* **2010**, *82*, 103011-1 – 103011-10.
22. Dutra, M., Lourenço, O., Avancini, S.S., Carlson, B.V., Delfino, A., Menezes, D.P., Providência, C., Typel, S., Stone, J.R., Relativistic mean-field hadronic models under nuclear matter constraints. *Phys. Rev. C*, **2014**, *90*, 055203-1 – 055203-35
23. Bednarek, I., Olchawa, W., Sładkowski, J., Syska, J., Regression analysis of the nuclear symmetry energy for relativistic mean-field models. *Phys. Rev. C*, **2022**, *106*, 055805-1–055805-24
24. Bednarek, I., Olchawa, W., Sładkowski, J., Syska, J., Relevance of the properties of nuclear matter to the radii of neutron stars, *Phys. Rev. C*, **2025**, *112*, 045806-1–045806-21
25. Bednarek, I., Olchawa, W., Sładkowski, J., Syska, J., A statistical approach to neutron stars' crust-core transition density and pressure. *Entropy*, **2023**, *25(12)*, 1652-1–1652-25
26. Bednarek, I., Olchawa, W., Sładkowski, J., Syska, J., Statistical analysis of the effect of the symmetry energy on the crust-core transition density and pressure in neutron stars. *Phys. Rev.C*,**2013**, *108*, 055801-1–055801-23

27. Stone, J.R. Stone, N.J., Moszkowski, S.A., Incompressibility in finite nuclei and nuclear matter. *Phys. Rev.C*, **2014**, *89*, 044316-1–25-044316
28. Khan, E., Margueron, J., Vidaña, I., Constraining the nuclear equation of state at subsaturation densities. *Phys. Rev. Lett.*, **2012**, *109*, 092501-1–092501-4
29. Khan, E., Margueron, J., Determination of the density dependence of the nuclear incompressibility. *Phys. Rev. C*, *2013*, *88*, 034319-1–034319-9
30. Li, B.A., Cai, B.J., Xie, W.J., Zhang, N.B., Progress in constraining nuclear symmetry energy using neutron star observables since GW170817. *Universe*, **2021**, *7(6)*, 182- – 182-39
31. Li, B.A., Han, X, Constraining the neutron–proton effective mass splitting using empirical constraints on the density dependence of nuclear symmetry energy around normal density. *Phys. Lett. B*, **2013**, *727*, 276 – 281
32. Oertel, M., Hempel, M., Klähn, T., Typel, S., Equations of state for supernovae and compact stars. *Rev. Mod. Phys.*, **2017**, *89*, 015007-1–015007-68
33. Mondal, C., Agrawal, B.K., De, J.N., Samaddar, S.K., Centelles, M., Viñas, X., Interdependence of different symmetry energy elements. *Phys. Rev. C*, **2017**, *96*, 021302-1–021302-5
34. Margueron, J., Casali, R.H., F. Gulminelli, F., Equation of state for dense nucleonic matter from metamodeling. II. Predictions for neutron star properties. *Phys. Rev. C*, **2018**, *97*, 025806 -1–025806-24
35. Kleinbaum, D.G., Kupper, L.L.; Nizam, A., Rosenberg, E.S., Applied Regression Analysis and Other Multivariable Methods. 5th ed.; Cengage Learning, Boston, USA, 2013, pp.61-64, 108-112.
36. Devore, J.L., Berk, K.N., Modern Mathematical Statistics with Applications. 2nd ed.; Springer New York Dordrecht Heidelberg London, 2012, pp.249 - 250, 654 - 658.